Benchmark: two Hybrid Mimetic Mixed schemes for the lid-driven cavity

Jérôme Droniou and Robert Eymard

Abstract We briefly present the Hybrid Mimetic Mixed scheme for the steady incompressible Navier-Stokes equations. Two centred approximations of the nonlinear convection term are proposed and compared, between themselves as well as with reference results from the literature, on the lid driven cavity test case applied to various grid types.

Key words: Hybrid Mimetic Mixed scheme, centred approximation, lid driven cavity

MSC (2010)**:** 65M60, 35Q30

1 Description of the scheme

The Hybrid Mimetic Mixed (HMM) methods [9] are a family of numerical methods for diffusion equations, that contains the Hybrid Finite Volume ("SUSHI") schemes [12], the mixed/hybrid Mimetic Finite Difference schemes [2] and the Mixed Finite Volume schemes [5]. We describe here their adaptation to Navier–Stokes equations in the case of homogeneous Dirichlet boundary conditions, that is, in their weak forms,

Jérôme Droniou
School of Mathematical Sciences, Monash University, Victoria 3800, Australia, e-mail: jerome.droniou@monash.edu

Robert Eymard
Laboratoire d'Analyse et de Mathématiques Appliquées, CNRS, UPEM, UPEC, 5 boulevard Descartes, Champs-sur-Marne 77454 Marne-la-Vallée Cedex 2, France. e-mail: Robert.Eymard@u-pem.fr

$$\begin{cases} \overline{u} \in \boldsymbol{H}^1_0(\Omega),\ \overline{p} \in L^2_0(\Omega), \\ \nu \displaystyle\int_\Omega \nabla\overline{u} : \nabla\overline{v}\,\mathrm{d}x + b(\overline{u},\overline{v}) - \int_\Omega \overline{p}\,\mathrm{div}\overline{v}\,\mathrm{d}x \\ \qquad\qquad = \displaystyle\int_\Omega (f\cdot\overline{v} + G : \nabla\overline{v})\,\mathrm{d}x,\ \forall \overline{v} \in \boldsymbol{H}^1_0(\Omega), \\ \displaystyle\int_\Omega q\,\mathrm{div}\overline{u}\,\mathrm{d}x = 0,\ \forall q \in L^2_0(\Omega). \end{cases} \tag{1}$$

Here, $\overline{u}$ and p represent the velocity field and the pressure, respectively. For a space E, we set $\boldsymbol{E} = E^d$. $L^2_0(\Omega)$ is the set of $L^2(\Omega)$ functions with zero average and, for all $\xi = (\xi_{i,j})_{i,j=1,\dots,d} \in \mathbb{R}^{d\times d}$ and $\chi = (\chi_{i,j})_{i,j=1,\dots,d} \in \mathbb{R}^{d\times d}$, $\xi : \chi = \sum_{i,j=1}^d \xi_{i,j}\chi_{i,j}$ is the doubly contracted product on $\mathbb{R}^{d\times d}$. The convection term is defined by

$$b(\overline{u},\overline{v}) = \sum_{i,j=1}^d \int_\Omega \overline{u}_i(x)\,\partial_i\overline{u}_j(x)\,\overline{v}_j(x)\,\mathrm{d}x,\ \forall \overline{u},\overline{v} \in \boldsymbol{H}^1_0(\Omega). \tag{2}$$

The assumptions on the domain, sources and viscosity are

$$\begin{array}{l} \Omega \text{ is an open bounded Lipschitz domain of } \mathbb{R}^d\ (d \in \{2,3\}), \\ f \in \boldsymbol{L}^2(\Omega) \text{ and } G \in \boldsymbol{L}^2(\Omega)^d,\ \nu > 0. \end{array} \tag{3}$$

The mixed/hybrid Mimetic Finite Difference schemes are, on triangular meshes and for particular choices of parameters, algebraically identical to the lowest order Raviart–Thomas method [14]. As a consequence, this $\mathbb{RT}_0$ scheme is a member of the HMM family of schemes. Since the hybridisation of $\mathbb{RT}_0$ gives the same matrix on the edge unknowns as the Crouzeix–Raviart scheme [4], and HMM methods are precisely hybrid schemes (with main unknowns on the edges), HMM is an extension to general polyhedral meshes of the Crouzeix–Raviart scheme.

The HMM scheme for (1) is given by

$$\begin{cases} u \in X_{D,0},\ p \in Y_{D,0}, \\ \nu \displaystyle\int_\Omega \nabla_D u : \nabla_D v\,\mathrm{d}x + b_D(u,v) - \int_\Omega \Theta_D p\ \mathrm{div}_D v\mathrm{d}x \\ \qquad\qquad = \displaystyle\int_\Omega (f\cdot \Pi_D v + G : \nabla_D v)\,\mathrm{d}x,\ \forall v \in X_{D,0}, \\ \displaystyle\int_\Omega \Theta_D q\,\mathrm{div}_D u\mathrm{d}x = 0,\ \ \forall q \in Y_{D,0}, \end{cases} \tag{4}$$

where the discrete spaces $X_{D,0}$, $Y_{D,0}$, the reconstruction operators ∇_D, Π_D, Θ_D and div_D, and the function b_D are described now.

1.1 The mesh

We consider polytopal meshes as in [8, Definition 7.2]. Let us recall the main elements and notations.

- $\mathcal{M}$ is a finite family of non empty connected open disjoint polytopal subsets of Ω (the "cells") such that $\overline{\Omega} = \cup_{K\in\mathcal{M}} \overline{K}$. For $K \in \mathcal{M}$ we denote by $|K| > 0$ and h_K the measure and diameter of K, respectively.
- $\mathcal{E} = \mathcal{E}_{\rm int} \cup \mathcal{E}_{\rm ext}$ is a finite family of disjoint hyperplanar subsets of $\overline{\Omega}$ (the "edges" of the mesh – "faces" in 3D), where $\mathcal{E}_{\rm int}$ is the set of edges included in Ω, and $\mathcal{E}_{\rm ext}$ is the set of edges included in $\partial\Omega$. The $(d-1)$-dimensional measure and the centre of gravity of $\sigma \in \mathcal{E}$ are respectively denoted by $|\sigma|$ and $\overline{x}_\sigma$.
  For $K \in \mathcal{M}$, $\mathcal{E}_K$ is the set of edges of K and, for $\sigma \in \mathcal{E}$, $\mathcal{M}_\sigma = \{K \in \mathcal{M} : \sigma \in \mathcal{E}_K\}$ is the set (made of one or two elements) of cells on each side of σ. If $\sigma \in \mathcal{E}_K$, $\mathbf{n}_{K,\sigma}$ is unit vector normal to σ outward to K.
- $\mathcal{P} = (x_K)_{K\in\mathcal{M}}$ is a family of points of Ω such that, for all $K \in \mathcal{M}$, K is strictly star-shaped with respect to x_K. $d_{K,\sigma}$ is the signed distance between x_K and the hyperplane containing σ, that is $d_{K,\sigma} = (x - x_K)\cdot\mathbf{n}_{K,\sigma}$ for any $x \in \sigma$. It is strictly positive due to K being strictly star-shaped with respect to x_K.

For all $K \in \mathcal{M}$ and $\sigma \in \mathcal{E}_K$, $D_{K,\sigma} = \{tx_K + (1-t)y : t \in (0,1),\ y \in \sigma\}$ is the cone with apex x_K and basis σ.

1.2 The gradient discretisation

The HMM method is a gradient discretisation method [10, 8, 7, 11]. As such, it is constructed through (4) by defining the discrete elements $D = (X_{D,0}, Y_{D,0}, \Pi_D, \Theta_D, \nabla_D, \mathrm{div}_D)$, together called a gradient discretisation.

- The space of discrete velocities, with zero boundary conditions, is $X_{D,0} = \{v = ((v_K)_{K\in\mathcal{M}}, (v_\sigma)_{\sigma\in\mathcal{E}}) : v_K \in \mathbb{R}^d, v_\sigma \in \mathbb{R}^d,\ v_\sigma = 0 \text{ for all } \sigma \in \mathcal{E}_{\rm ext}\}$.
- The space of the discrete pressures, with zero average value, is $Y_{D,0} = \{q = (q_K)_{K\in\mathcal{M}} : q_K \in \mathbb{R},\ \sum_{K\in\mathcal{M}} |K| q_K = 0\}$.

Thus, the velocity is approximated by one vector in each cell and one vector on each interior edge, while the pressure is approximated by one scalar unknown in each cell.

- The linear mapping $\Pi_D : X_{D,0} \to \boldsymbol{L}^2(\Omega)$ is the nonconforming piecewise constant reconstruction in the control volumes of the complete velocity, defined by
$$\forall v \in X_{D,0},\ \forall K \in \mathcal{M},\ \Pi_D v = v_K \text{ on } K.$$
- The linear mapping $\Theta_D : Y_{D,0} \to L^2(\Omega)$ is similarly defined by
$$\forall q \in Y_{D,0},\ \forall K \in \mathcal{M},\ \Theta_D q = q_K \text{ on } K.$$
  Notice that $\int_\Omega \Theta_D q \mathrm{d}x = 0$ for all $q \in Y_{D,0}$.
- The piecewise constant gradient reconstruction $\nabla_D : X_{D,0} \to \boldsymbol{L}^2(\Omega)^d$ is given by

$$\forall K \in \mathscr{M}, \forall \sigma \in \mathscr{E}_K, \forall x \in D_{K,\sigma},$$
$$\nabla_D v(x) = \overline{\nabla}_K v + \frac{\sqrt{d}}{d_{K,\sigma}} (v_\sigma - v_K - (\overline{\nabla}_K v)(\overline{x}_\sigma - x_K)) \otimes \mathbf{n}_{K,\sigma},$$

where $\overline{\nabla}_K v = \frac{1}{|K|} \sum_{\sigma \in \mathscr{E}_K} |\sigma| v_\sigma \otimes \mathbf{n}_{K,\sigma}$. Note that this reconstructed gradient is one possible choice, corresponding to the SUSHI method [12], in the entire family of HMM methods [8, 10].

- The linear divergence reconstruction $\mathrm{div}_D : X_{D,0} \to L^2(\Omega)$ is defined by

$$\forall v \in X_{D,0}, \forall K \in \mathscr{M}, \forall x \in K, \mathrm{div}_D v(x) = \frac{1}{|K|} \sum_{\sigma \in \mathscr{E}_K} |\sigma| v_\sigma \cdot \mathbf{n}_{K,\sigma} = \frac{1}{|K|} \int_K \mathrm{Tr}(\nabla_D v).$$

The last equality is a consequence of [8, Eq. (12.10)] which shows that the average over K of $\nabla_D v$ is $\overline{\nabla}_K v$.

1.3 The discrete convection term

We compare two expressions for the discrete convection term, respectively denoted by (c1) and (c2).

1.3.1 Version (c1): centred using cell values

A first centred version of the convection term $b_D(u,v)$ is computed from cell and face discrete velocities by:

$$b_D(u,v) = \sum_{\sigma \in \mathscr{E}_{\mathrm{int}}, \mathscr{M}_\sigma = \{K,L\}} |\sigma| \, u_\sigma \cdot \mathbf{n}_{K,\sigma} \, (u_L - u_K) \cdot \frac{v_K + v_L}{2}. \tag{c1}$$

The proof of convergence of (4) with the choice (c1) can be found in [6].

Remark 1. Although not considered in the numerical tests below, an upstream weighted version of (c1) can easily be written:

$$b_D^{(\mathrm{up})}(u,v) = \sum_{\sigma \in \mathscr{E}_{\mathrm{int}}, \mathscr{M}_\sigma = \{K,L\}} |\sigma| ((u_\sigma \cdot \mathbf{n}_{K,\sigma})^+ v_K - (u_\sigma \cdot \mathbf{n}_{K,\sigma})^- v_L) \cdot (u_L - u_K).$$

1.3.2 Version (c2): centred using local edge values

A second centred version of the convection term $b_D(u,v)$ (inspired by [13]) is locally computed using only the discrete velocities on the internal faces. We write $b_D(u,v) = \sum_{K \in \mathscr{M}} b_K(u,v)$ and compute local contributions $b_K(u,v)$ by using only values on the edges of K. We present the construction in the 2D case. The idea is

to split the cell K into sub-triangles, to introduce fluxes on the edges of these triangles that are internal to K, and to use these fluxes to write a centered discretisation on the sub-triangulation – by assuming that u takes the value u_σ on the triangle corresponding to σ.

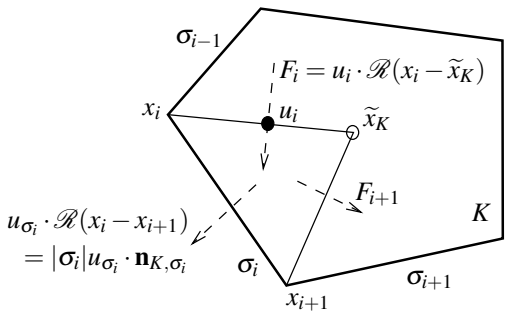

Fig. 1 Construction of the centered scheme (c2): subdivision of K and internal fluxes.

Following the notations in Fig. 1, let $\widetilde{x}_K$ be the barycentre of all vertices $(x_i)_{i=1,n}$ of K, numbered in the direct trigonometric order. The internal edges are the segments $[\widetilde{x}_K, x_i]$ for all $i = 1, \ldots, n$. We consider a family of velocities $(u_i)_{i=1,\ldots,n}$ on these internal edges and we set the internal fluxes $F_i = u_i \cdot \mathscr{R}(x_i - \widetilde{x}_K)$, where $\mathscr{R}$ is the direct rotation with angle $\frac{\pi}{2}$. These velocities are constructed such that the divergence-free property is satisfied on each sub-triangle, that is

$$F_{i+1} - F_i + u_{\sigma_i} \cdot \mathscr{R}(x_i - x_{i+1}) = 0, \ \forall i = 1, \ldots, n. \tag{5}$$

Then we set

$$\begin{aligned} b_K(u,v) &= \sum_{i=1}^{n} F_i (u_{\sigma_i} - u_{\sigma_{i-1}}) \cdot \frac{v_{\sigma_i} + v_{\sigma_{i-1}}}{2} \\ &= \sum_{i=1}^{n} u_i \cdot \mathscr{R}(x_i - \widetilde{x}_K)(u_{\sigma_i} - u_{\sigma_{i-1}}) \cdot \frac{v_{\sigma_i} + v_{\sigma_{i-1}}}{2}. \end{aligned} \tag{c2}$$

Note that the terms corresponding to fluxes across each σ_i do not appear here. Indeed, with our approximation of u by u_σ in the two sub-triangles in the cells on both sides of σ, these terms would involve the vanishing quantity $u_{\sigma_i} - u_{\sigma_i}$. Or course, the value u_{σ_i} itself has a direct influence on the internal fluxes $(F_j)_{j=1,\ldots,n}$ that are involved in (c2).

For the practical implementation, we remark that only the fluxes $(F_i)_{i=1,\ldots,n}$ are required, the complete velocities $(u_i)_{i=1,\ldots,n}$ do not need to be known. The linear system (5) on $(F_i)_{i=1,\ldots,n}$ has n equations and rank $n-1$. To solve this system, we choose the complementary relation

$$\sum_{i=1}^{n} F_i = \sum_{i=1}^{n} u_i \cdot \mathscr{R}(x_i - \widetilde{x}_K) = 0. \tag{6}$$

Using this relation, we obtain values F_i that are consistent at the first order (since $\sum_{i=1}^{n}(x_i - \widetilde{x}_K) = 0$), that is to say, exact fluxes coming from a constant velocity satisfy (5)–(6).

Remark 2 (Computational costs). The centered version (c1) has a major drawback when it comes to solving the numerical systems involved in the Newton iterations. Indeed, these systems have cell-cell connectivities in their stencil and the total number of unknowns is $2 \times \sharp$internal edges $+ 3 \times \sharp$cells (edge velocities, cell velocities and cell pressures). The version (c2) behaves much better. Only cell-edges connectivities are involved and, as in the HMM method for pure diffusion, velocity cell unknowns can be locally eliminated by static condensation, using only the edges around each cell. After performing these eliminations, the global system to be solved only has $2 \times \sharp$internal edges $+ \sharp$cells unknowns (edge velocities and cell pressures). This is why, in the following tests, we were able to run (c2), contrary to (c1), on the thinnest meshes. Tables 1 and 2 give a more precise idea of the complexity of (c1) and (c2) on triangular and quadrangular meshes.

Remark 3. As for the (c1) formulation, an upstream weighted formulation could be considered as well, with the same advantage with respect to the reduced stencil:

$$b_K^{(\mathrm{up})}(u,v) = \sum_{i=1}^{n} (F_i^+ v_{\sigma_i} - F_i^- v_{\sigma_{i-1}}) \cdot (u_{\sigma_i} - u_{\sigma_{i-1}}).$$

2 Numerical results on the 2D lid driven cavity

This classical test case is described in [1, Case 6]. We present the results provided by the HMM method with the two centered discretisations (c1) and (c2) described in Section 1.3. The non-linear system (4) was solved using a sub-relaxed Newton algorithm with a tolerance of 10^{-5} on the infinity norm of the velocity. At each iteration, the linear system is solved with the `hsl_ma48` routine of the HSL library ([1]). The choice of the sub-relaxation was not optimised but nearly all the tests converged in about 22 Newton iterations. For the reasons explained in Remark 2, the version (c1) was not run on the meshes `quad6` and `quad7`, as the linear solver is too slow given size and stencil of the matrices involved for these meshes.

Although we run the tests for all mesh families and all Reynolds numbers, we only report here the results for the quadrangular and triangular meshes (except for one comparison with the locally refined meshes). While comparing these results between the two families of meshes, the following needs to be taken into account. Considering the case of (c2), as explained in Remark 2 the final number of DOFs

[1] `http://www.hsl.rl.ac.uk/`

is $2 \times \sharp$internal edges $+ \sharp$cells. Tables 1 and 2 give an idea of the complexity of the method applied to some meshes of the triangular and quadrangular families, using the notations in [1]: **nuu** is the number of velocity unknowns, **npu** is the number of pressure unknowns, **nnzu** is the number of non-zero terms in the velocity–velocity matrix, and **nnzup** is the number of non-zero terms in the velocity–pressure matrix. The orders of magnitude of the numbers of unknowns show that a fair comparison between triangular and quadrangular meshes needs to be done by looking in parallel at the results of `tri`i and `quad`$(i+1)$ (with, even then, an expected slight advantage for triangular meshes).

mesh	**nuu**	**npu**	**nnzu**	**nnzup**	**nuu+npu**
`tri1`	184	40	1824	208	224
`tri2`	1084	224	11608	1272	1308
`tri3`	4594	934	50328	5452	5528
`tri4`	31914	6422	354536	38140	38336
`tri5`	128964	25872	1438536	154440	154836
`tri6`	521304	104420	5826824	624928	625724
`quad1`	80	16	928	96	96
`quad2`	352	64	4704	448	416
`quad3`	1472	256	20896	1920	1728
`quad4`	6016	1024	87840	7936	7040
`quad5`	24320	4096	359968	32256	28416
`quad6`	97792	16384	1457184	130048	114176
`quad7`	392192	65536	5863456	522240	457728

Table 1 Complexity table for (c1) on triangular and quadrangular meshes.

mesh	**nuu**	**npu**	**nnzu**	**nnzup**	**nuu+npu**
`tri1`	104	40	912	208	144
`tri2`	636	224	6072	1272	860
`tri3`	2726	934	26652	5452	3660
`tri4`	19070	6422	189132	38140	25492
`tri5`	77220	25872	769032	154440	103092
`tri6`	312464	104420	3118272	624928	416884
`quad1`	48	16	512	96	64
`quad2`	224	64	2784	448	288
`quad3`	960	256	12704	1920	1216
`quad4`	3968	1024	54048	7936	4992
`quad5`	16128	4096	222752	32256	20224
`quad6`	65024	16384	904224	130048	81408
`quad7`	261120	65536	3643424	522240	326656

Table 2 Complexity table for (c2) on triangular and quadrangular meshes.

2.1 High Reynolds numbers: $\mathrm{Re} = 1000$ *and* $\mathrm{Re} = 5000$

- $\mathrm{Re} = 1000$ ($\nu = 0.0001$): see Tables 3, 4, 5, 6, 7, 8, 9, and Fig. 2.
- $\mathrm{Re} = 5000$ ($\nu = 0.0002$): see Tables 10, 11, and Fig. 3 and 4.

For comparison purposes, we recall in these tables the results in [3], modified by symmetry with respect to the vertical midline (due to the choice of an opposite velocity on the lid). These results are obtained on very thin meshes (1024×1024 Cartesian mesh) with a third order scheme.

mesh #	$x_{\min}$	$y_{\min}$	$\psi_{\min}$	$x_{\max}$	$y_{\max}$	$\psi_{\max}$
1	0.721	0.721	$-2.66\cdot10^{-2}$	0.000	0.750	$1.1\cdot10^{-17}$
2	0.653	0.781	$-3.97\cdot10^{-2}$	0.000	0.889	$3.47\cdot10^{-18}$
3	0.590	0.628	$-5.69\cdot10^{-2}$	0.870	0.187	$8.98\cdot10^{-4}$
4	0.533	0.576	$-9.02\cdot10^{-2}$	0.862	0.130	$1.52\cdot10^{-3}$
5	0.530	0.566	-0.108	0.861	0.110	$1.63\cdot10^{-3}$
6	0.531	0.566	-0.116	0.863	0.113	$1.7\cdot10^{-3}$

mesh #	$x_{\min}$	$y_{\min}$	$\psi_{\min}$	$x_{\max}$	$y_{\max}$	$\psi_{\max}$
1	0.501	0.499	$-2.24\cdot10^{-2}$	0.000	0.750	$1.84\cdot10^{-18}$
2	0.633	0.645	$-5.77\cdot10^{-2}$	0.000	0.889	$3.47\cdot10^{-18}$
3	0.590	0.628	$-8.72\cdot10^{-2}$	0.883	0.147	$1.32\cdot10^{-3}$
4	0.533	0.576	-0.111	0.862	0.130	$1.93\cdot10^{-3}$
5	0.530	0.566	-0.118	0.861	0.110	$1.79\cdot10^{-3}$
6	0.531	0.566	-0.119	0.863	0.114	$1.75\cdot10^{-3}$

	$x_{\min}$	$y_{\min}$	$\psi_{\min}$	$x_{\max}$	$y_{\max}$	$\psi_{\max}$
[3]	0.53125	0.56543	-0.11892	0.86328	0.1123	$1.7292\cdot10^{-3}$

Table 3 Stream function table : Triangular meshes, $\nu = 1/1000$ (top to bottom: (c1), (c2), ref.)

mesh #	$x_{\min}$	$y_{\min}$	$\psi_{\min}$	$x_{\max}$	$y_{\max}$	$\psi_{\max}$
1	0.530	0.755	$-1.87\cdot10^{-2}$	1.000	1.000	$9.64\cdot10^{-18}$
2	0.639	0.747	$-2.73\cdot10^{-2}$	1.000	1.000	$9\cdot10^{-18}$
3	0.683	0.746	$-3.76\cdot10^{-2}$	$5.89\cdot10^{-2}$	$5.01\cdot10^{-2}$	$4.17\cdot10^{-5}$
4	0.565	0.623	$-5.58\cdot10^{-2}$	0.874	0.126	$7.71\cdot10^{-4}$
5	0.548	0.593	$-7.8\cdot10^{-2}$	0.861	0.124	$1.41\cdot10^{-3}$

mesh #	$x_{\min}$	$y_{\min}$	$\psi_{\min}$	$x_{\max}$	$y_{\max}$	$\psi_{\max}$
1	0.530	0.755	$-1.58\cdot10^{-2}$	1.000	1.000	0.000
2	0.760	0.771	$-2.83\cdot10^{-2}$	0.866	0.123	$9.75\cdot10^{-5}$
3	0.625	0.635	$-4.21\cdot10^{-2}$	0.862	0.134	$5.54\cdot10^{-4}$
4	0.531	0.600	$-6.46\cdot10^{-2}$	0.837	0.152	$1.6\cdot10^{-3}$
5	0.533	0.578	$-8.88\cdot10^{-2}$	0.861	0.124	$1.57\cdot10^{-3}$
6	0.532	0.570	-0.107	0.867	0.117	$1.64\cdot10^{-3}$
7	0.531	0.567	-0.115	0.864	0.113	$1.7\cdot10^{-3}$

	$x_{\min}$	$y_{\min}$	$\psi_{\min}$	$x_{\max}$	$y_{\max}$	$\psi_{\max}$
[3]	0.53125	0.56543	-0.11892	0.86328	0.1123	$1.7292\cdot10^{-3}$

Table 4 Stream function table : Quadrangular meshes, $\nu = 1/1000$ (top to bottom: (c1), (c2), ref.)

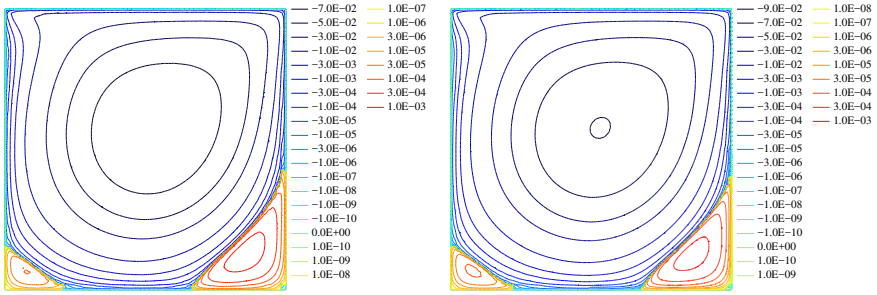

Fig. 2 Streamlines for $\nu = 1/1000$ using (c2) (left: mesh `quad5`; right: mesh `ref5`).

mesh #	$x_{\min}$	$y_{\min}$	$\psi_{\min}$	$x_{\max}$	$y_{\max}$	$\psi_{\max}$
1	0.500	0.750	$-1.52 \cdot 10^{-2}$	0.875	0.500	$3.02 \cdot 10^{-3}$
2	0.625	0.750	$-2.63 \cdot 10^{-2}$	0.969	$3.12 \cdot 10^{-2}$	$4.23 \cdot 10^{-6}$
3	0.625	0.688	$-3.78 \cdot 10^{-2}$	$6.25 \cdot 10^{-2}$	$6.25 \cdot 10^{-2}$	$5.34 \cdot 10^{-5}$
4	0.562	0.625	$-5.55 \cdot 10^{-2}$	0.875	0.125	$5.06 \cdot 10^{-4}$
5	0.531	0.578	$-7.95 \cdot 10^{-2}$	0.863	0.121	$1.16 \cdot 10^{-3}$

mesh #	$x_{\min}$	$y_{\min}$	$\psi_{\min}$	$x_{\max}$	$y_{\max}$	$\psi_{\max}$
1	0.625	0.500	$-1.44 \cdot 10^{-2}$	0.000	0.750	$8.67 \cdot 10^{-19}$
2	0.625	0.625	$-2.6 \cdot 10^{-2}$	0.938	$9.38 \cdot 10^{-2}$	$3.41 \cdot 10^{-5}$
3	0.562	0.625	$-4.29 \cdot 10^{-2}$	0.875	0.141	$4.51 \cdot 10^{-4}$
4	0.531	0.594	$-6.59 \cdot 10^{-2}$	0.836	0.141	$1.33 \cdot 10^{-3}$
5	0.531	0.578	$-9.05 \cdot 10^{-2}$	0.859	0.121	$1.43 \cdot 10^{-3}$

	$x_{\min}$	$y_{\min}$	$\psi_{\min}$	$x_{\max}$	$y_{\max}$	$\psi_{\max}$
[3]	0.53125	0.56543	-0.11892	0.86328	0.1123	$1.7292 \cdot 10^{-3}$

Table 5 Stream function table : Locally refined meshes, $\nu = 1/1000$ (top to bottom: (c1), (c2), ref.)

The stream functions tables clearly show that (c2) outperforms (c1) in all instances, for coarse as well as thin meshes. The difference between these two schemes is less prominent on triangular meshes, but it is rather noticeable on quadrangular meshes (and locally refined meshes) – including the thinnest ones. Even on meshes coarser than in [3], we notice that (c2) provides comparable results regarding the location and values of the minimum and maximum of the stream function. The velocity values are a bit off, but not by much: no more than 2% on `tri6` and no more than 5% on `quad7` (note that [3] does not provide velocity values for $\mathrm{Re} = 5000$, which is why our own velocity values for this Reynolds number are not represented here).

Bearing in mind the discussion in Section 2 concerning the numbers of DOFs, it seems that (c2) performs equally well on triangular and quadrangular meshes. This shows the efficiency of HMM, alongside a proper discretisation of the convection term, to tackle meshes of varied geometry. The results obtained on the stream func-

tion with the locally refined meshes are slightly less accurate than the one with the quadrangles, but they remain acceptable (note that the locally refined mesh `ref5` leads to about 50,000 DOFs, which puts it in between `quad5` and `quad6` in terms of computational cost).

Mesh #	y	0.0000	0.0625	0.1016	0.2813	0.5000	0.7344	0.9531	0.9688	1.0000
1		0.0000	−0.0087	−0.0142	−0.0140	0.0163	0.0902	0.7820	0.8550	1.0000
2		0.0003	−0.0366	−0.0526	−0.0736	−0.0481	−0.0014	0.4330	0.5140	1.0300
3		−0.0001	−0.0345	−0.0616	−0.1610	−0.0658	0.0471	0.4410	0.5520	1.0100
4		0.0001	−0.1260	−0.1960	−0.2360	−0.0501	0.1200	0.4140	0.5430	0.9990
5		0.0001	−0.1800	−0.2680	−0.2570	−0.0551	0.1600	0.4500	0.5720	0.9990
6		0.0000	−0.1960	−0.2920	−0.2730	−0.0598	0.1800	0.4650	0.5770	1.0000

Mesh #	y	0.0000	0.0625	0.1016	0.2813	0.5000	0.7344	0.9531	0.9688	1.0000
1		0.0000	−0.0099	−0.0161	−0.0202	0.0045	0.0555	0.7720	0.8480	1.0000
2		0.0002	−0.0582	−0.0836	−0.1080	−0.0796	0.0244	0.6050	0.6500	1.0100
3		−0.0002	−0.0661	−0.1080	−0.2230	−0.1270	0.0830	0.5450	0.6760	0.9830
4		0.0001	−0.1490	−0.2320	−0.2940	−0.0673	0.1600	0.5090	0.6400	0.9990
5		0.0001	−0.1920	−0.2880	−0.2840	−0.0626	0.1810	0.4910	0.6190	0.9990
6		0.0000	−0.2000	−0.2980	−0.2810	−0.0623	0.1870	0.4760	0.5900	1.0000

y	0.0000	0.0625	0.1016	0.2813	0.5000	0.7344	0.9531	0.9688	1.0000
[3]	0.0000	-0.20227	-0.30029	-0.28040	-0.06205	0.18861	0.47239	0.58031	1.0000

Table 6 Hor. velocity $y \mapsto u(0.5,y)$: Triangular meshes, $\nu = 1/1000$ (top to bottom: (c1), (c2), ref.)

Mesh #	x	0.0000	0.0703	0.0938	0.2266	0.5000	0.8594	0.9453	0.9609	1.0000
1		0.0000	0.0098	0.0131	0.0204	−0.0265	0.0007	0.0003	0.0002	0.0000
2		−0.0004	0.0546	0.0657	0.0706	0.0160	−0.1290	−0.1120	−0.1000	0.0034
3		−0.0007	0.1040	0.1180	0.1430	0.0213	−0.2280	−0.1230	−0.0959	0.0022
4		−0.0004	0.2220	0.2500	0.2550	0.0167	−0.3820	−0.2640	−0.1790	−0.0002
5		−0.0001	0.2710	0.3050	0.3040	0.0222	−0.4090	−0.3630	−0.2560	−0.0005
6		0.0000	0.2890	0.3250	0.3250	0.0246	−0.4210	−0.3980	−0.2830	0.0000

Mesh #	x	0.0000	0.0703	0.0938	0.2266	0.5000	0.8594	0.9453	0.9609	1.0000
1		0.0000	0.0054	0.0072	0.0125	−0.0031	−0.0136	−0.0053	−0.0038	0.0000
2		−0.0009	0.0772	0.0906	0.1020	0.0138	−0.1980	−0.1810	−0.1690	0.0037
3		−0.0029	0.1440	0.1680	0.2040	0.0413	−0.3200	−0.2150	−0.1650	0.0020
4		−0.0003	0.2640	0.2940	0.3130	0.0225	−0.4490	−0.3310	−0.2330	−0.0003
5		−0.0001	0.2930	0.3280	0.3320	0.0248	−0.4390	−0.3970	−0.2850	−0.0006
6		0.0000	0.2960	0.3320	0.3340	0.0253	−0.4300	−0.4070	−0.2910	0.0000

x	0.0000	0.0703	0.0938	0.2266	0.5000	0.8594	0.9453	0.9609	1.0000
[3]	0.0000	0.29622	0.33290	0.33398	0.02580	-0.42634	-0.41018	-0.29330	0.0000

Table 7 Ver. velocity $x \mapsto v(x,0.5)$: Triangular meshes, $\nu = 1/1000$ (top to bottom: (c1), (c2), ref.)

Remark 4. In the velocity tables for triangular meshes (Tables 6 and 7), the boundary conditions at $x,y = 0$ and $x,y = 1$ are not perfectly represented due to our choice of interpolation. In the HMM method, the velocity is represented by values at the cell

centers and a the midpoints of the edges; to obtain values at $x = 0.5$ or $y = 0.5$, we had to interpolate the cell/edge values around the required points. Of course, we could have manually adjusted the interpolation rules at the domain's boundary to ensure that the boundary conditions were respected, but we decided for consistency to use the same interpolation procedures inside the domain and on the boundary.

Mesh #	y	0.0000	0.0625	0.1016	0.2813	0.5000	0.7344	0.9531	0.9688	1.0000
1		0.0000	0.0125	0.0098	0.0103	0.0352	0.0843	0.7300	0.7890	1.0000
2		0.0000	−0.0233	−0.0370	−0.0337	−0.0211	−0.0043	0.6380	0.7470	1.0000
3		0.0000	−0.0422	−0.0570	−0.0730	−0.0433	0.0004	0.3540	0.5510	1.0000
4		0.0000	−0.0577	−0.0864	−0.1510	−0.0506	0.0480	0.3780	0.5070	1.0000
5		0.0000	−0.1050	−0.1610	−0.2140	−0.0444	0.0954	0.3700	0.5130	1.0000

Mesh #	y	0.0000	0.0625	0.1016	0.2813	0.5000	0.7344	0.9531	0.9688	1.0000
1		0.0000	−0.0088	−0.0133	−0.0202	0.0003	0.0814	0.7700	0.8280	1.0000
2		0.0000	−0.0083	−0.0137	−0.0612	−0.0640	0.0032	0.6530	0.7620	1.0000
3		0.0000	−0.0208	−0.0364	−0.1090	−0.0658	0.0315	0.3730	0.5750	1.0000
4		0.0000	−0.0375	−0.0725	−0.2090	−0.0552	0.0695	0.3630	0.4900	1.0000
5		0.0000	−0.1200	−0.1900	−0.2360	−0.0497	0.1190	0.3970	0.5290	1.0000
6		0.0000	−0.1750	−0.2630	−0.2570	−0.0554	0.1590	0.4430	0.5610	1.0000
7		0.0000	−0.1950	−0.2900	−0.2720	−0.0598	0.1790	0.4640	0.5750	1.0000

y	0.0000	0.0625	0.1016	0.2813	0.5000	0.7344	0.9531	0.9688	1.0000
[3]	0.0000	-0.20227	-0.30029	-0.28040	-0.06205	0.18861	0.47239	0.58031	1.0000

Table 8 Hor. velocity $y \mapsto u(0.5, y)$: Quadrangular meshes, $\nu = 1/1000$ (top to bottom: (c1), (c2), ref.)

Mesh #	x	0.0000	0.0703	0.0938	0.2266	0.5000	0.8594	0.9453	0.9609	1.0000
1		0.0000	0.0031	0.0048	0.0143	0.0077	−0.0180	−0.0071	−0.0050	0.0000
2		0.0000	0.0226	0.0288	0.0356	0.0098	−0.0446	−0.0228	−0.0181	0.0000
3		0.0000	0.0526	0.0600	0.0683	0.0192	−0.1220	−0.1150	−0.0817	0.0000
4		0.0000	0.1110	0.1260	0.1330	0.0234	−0.2310	−0.1520	−0.1090	0.0000
5		0.0000	0.1880	0.2110	0.2190	0.0161	−0.3410	−0.2230	−0.1500	0.0000

Mesh #	x	0.0000	0.0703	0.0938	0.2266	0.5000	0.8594	0.9453	0.9609	1.0000
1		0.0000	0.0061	0.0087	0.0232	0.0007	−0.0367	−0.0144	−0.0106	0.0000
2		0.0000	0.0240	0.0303	0.0338	−0.0125	−0.0685	−0.0320	−0.0255	0.0000
3		0.0000	0.0630	0.0713	0.0823	0.0137	−0.1520	−0.0873	−0.0610	0.0000
4		0.0000	0.1400	0.1570	0.1670	0.0118	−0.2900	−0.1300	−0.0843	0.0000
5		0.0000	0.2190	0.2460	0.2510	0.0153	−0.3820	−0.2550	−0.1720	0.0000
6		0.0000	0.2680	0.3010	0.3020	0.0216	−0.4070	−0.3560	−0.2490	0.0000
7		0.0000	0.2880	0.3240	0.3240	0.0245	−0.4200	−0.3950	−0.2810	0.0000

x	0.0000	0.0703	0.0938	0.2266	0.5000	0.8594	0.9453	0.9609	1.0000
[3]	0.0000	0.29622	0.33290	0.33398	0.02580	-0.42634	-0.41018	-0.29330	0.0000

Table 9 Ver. velocity $x \mapsto v(x, 0.5)$: Quadrangular meshes, $\nu = 1/1000$ (top to bottom: (c1), (c2), ref.)

Qualitatively speaking, (c2) also seems to provide more accurate results than (c1) on the streamlines. Comparing both pictures in Fig. 3, we see that (c2) starts

mesh #	$x_{\min}$	$y_{\min}$	$\psi_{\min}$	$x_{\max}$	$y_{\max}$	$\psi_{\max}$
1	0.721	0.721	$-1.09\cdot10^{-2}$	0.000	0.750	$7.91\cdot10^{-18}$
2	0.655	0.849	$-1.68\cdot10^{-2}$	0.000	0.889	$3.47\cdot10^{-18}$
3	0.594	0.583	$-2.47\cdot10^{-2}$	0.905	$9.35\cdot10^{-2}$	$1.15\cdot10^{-4}$
4	0.512	0.571	$-4.24\cdot10^{-2}$	0.802	0.101	$1.82\cdot10^{-3}$
5	0.515	0.540	$-6.52\cdot10^{-2}$	0.818	$8.26\cdot10^{-2}$	$2.19\cdot10^{-3}$
6	0.518	0.535	$-8.92\cdot10^{-2}$	0.817	$7.49\cdot10^{-2}$	$2.64\cdot10^{-3}$

mesh #	$x_{\min}$	$y_{\min}$	$\psi_{\min}$	$x_{\max}$	$y_{\max}$	$\psi_{\max}$
1	0.279	0.721	$-8.18\cdot10^{-3}$	0.000	0.750	$1.73\cdot10^{-18}$
2	0.633	0.645	$-2.84\cdot10^{-2}$	0.000	0.889	$1.39\cdot10^{-17}$
3	0.594	0.583	$-5.23\cdot10^{-2}$	$5.4\cdot10^{-2}$	$5.38\cdot10^{-2}$	$1.08\cdot10^{-4}$
4	0.533	0.576	$-8.91\cdot10^{-2}$	0.771	0.110	$4.56\cdot10^{-3}$
5	0.521	0.546	-0.112	0.795	$7.81\cdot10^{-2}$	$3.64\cdot10^{-3}$
6	0.515	0.539	-0.121	0.802	$7.06\cdot10^{-2}$	$3.44\cdot10^{-3}$

	$x_{\min}$	$y_{\min}$	$\psi_{\min}$	$x_{\max}$	$y_{\max}$	$\psi_{\max}$
[3]	0.51465	0.53516	-0.12191	0.80566	0.073242	$3.0694\cdot10^{-3}$

Table 10 Stream function table : Triangular meshes, $\nu = 1/5000$ (top to bottom: (c1), (c2), ref.)

mesh #	$x_{\min}$	$y_{\min}$	$\psi_{\min}$	$x_{\max}$	$y_{\max}$	$\psi_{\max}$
1	0.530	0.755	$-8.44\cdot10^{-3}$	1.000	1.000	$4.32\cdot10^{-18}$
2	0.489	0.865	$-1.05\cdot10^{-2}$	1.000	1.000	$4.09\cdot10^{-18}$
3	0.693	0.865	$-1.63\cdot10^{-2}$	$5.89\cdot10^{-2}$	$5.01\cdot10^{-2}$	$3.98\cdot10^{-5}$
4	0.618	0.593	$-2.31\cdot10^{-2}$	0.943	0.118	$2.22\cdot10^{-4}$
5	0.531	0.564	$-3.35\cdot10^{-2}$	0.827	0.109	$1.43\cdot10^{-3}$

mesh #	$x_{\min}$	$y_{\min}$	$\psi_{\min}$	$x_{\max}$	$y_{\max}$	$\psi_{\max}$
1	0.787	0.481	$-7.15\cdot10^{-3}$	1.000	1.000	0.000
2	0.760	0.771	$-1.07\cdot10^{-2}$	1.000	1.000	$1.84\cdot10^{-18}$
3	0.611	0.679	$-1.34\cdot10^{-2}$	0.823	0.177	$3.07\cdot10^{-4}$
4	0.526	0.570	$-2.75\cdot10^{-2}$	0.747	0.124	$1.51\cdot10^{-3}$
5	0.517	0.548	$-4.23\cdot10^{-2}$	0.811	0.109	$1.92\cdot10^{-3}$
6	0.516	0.539	$-6.44\cdot10^{-2}$	0.820	$8.53\cdot10^{-2}$	$2.19\cdot10^{-3}$
7	0.516	0.536	$-8.83\cdot10^{-2}$	0.816	$7.82\cdot10^{-2}$	$2.61\cdot10^{-3}$

	$x_{\min}$	$y_{\min}$	$\psi_{\min}$	$x_{\max}$	$y_{\max}$	$\psi_{\max}$
[3]	0.51465	0.53516	-0.12191	0.80566	0.073242	$3.0694\cdot10^{-3}$

Table 11 Stream function table : Quadrangular meshes, $\nu = 1/5000$ (top to bottom: (c1), (c2), ref.)

to captures already on `quad5` the third vortex (in the upper left corner), whereas (c1) fails to represent it. This vortex appears even more clearly using `quad6` and `quad7` (see Fig. 4).

2.2 Low Reynolds numbers: $\mathrm{Re} = 100$ *and* $\mathrm{Re} = 400$

- $\mathrm{Re} = 100$ ($\nu = 0.01$): see Tables 12, 13 and Fig. 5.
- $\mathrm{Re} = 400$ ($\nu = 0.0025$): see Tables 14, 15 and Fig. 6.

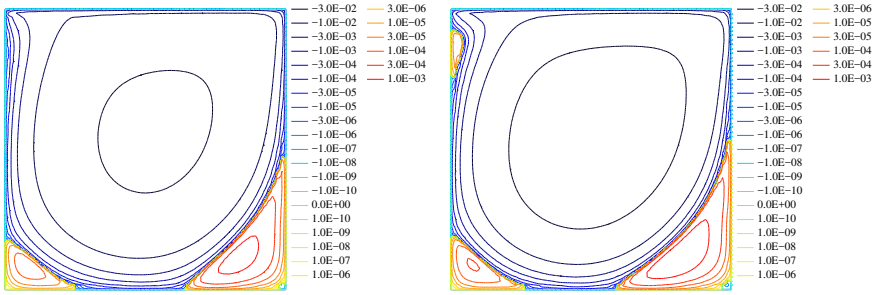

Fig. 3 Streamlines for $\nu = 1/5000$ on the mesh `quad5` (left: (c1); right: (c2)).

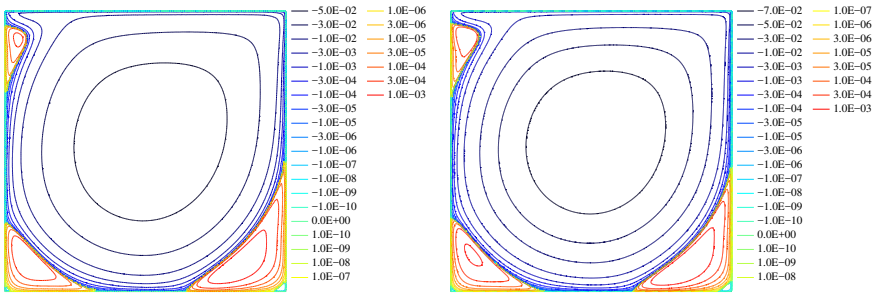

Fig. 4 Streamlines for $\nu = 1/5000$ using (c2) (left: mesh `quad6`; right: mesh `quad7`).

For Reynolds numbers of 100 and 400, the literature does not seem to contain results to which we can precisely compare our outputs. The general comment we can however make is that, as for high Reynolds numbers, the HMM method seems to perform equally well on triangles and quadrangles (with comparable numbers of DOFs), and that (c2) still outperforms (c1) on quadrangular meshes. On triangular meshes, the difference between (c1) and (c2) seems to be smeared out compared to the case of high Reynolds numbers.

3 Conclusion

An advantage of the HMM scheme for the Navier–Stokes equations is that it applies on every type of polyhedral mesh, which can be helpful in the case of domains with complex geometry. It can actually be considered as an extension of the Crouzeix–Raviart scheme to general meshes. In this paper, two different formulations for the convection term were tested, showing a clear advantage, from the accuracy point of view, to the version which also has the cheapest computational cost (i.e. convection term (c2)). A very good agreement is obtained, using this formulation, between the

mesh #	$x_{\min}$	$y_{\min}$	$\psi_{\min}$	$x_{\max}$	$y_{\max}$	$\psi_{\max}$
1	0.721	0.721	$-6.91\cdot10^{-2}$	0.000	0.750	$2.6\cdot10^{-17}$
2	0.598	0.731	$-9.17\cdot10^{-2}$	0.908	$9.16\cdot10^{-2}$	$5.92\cdot10^{-5}$
3	0.611	0.759	$-9.94\cdot10^{-2}$	0.960	$9\cdot10^{-2}$	$2.93\cdot10^{-5}$
4	0.614	0.731	-0.103	0.941	$5.9\cdot10^{-2}$	$1.57\cdot10^{-5}$
5	0.614	0.741	-0.103	0.941	$5.82\cdot10^{-2}$	$1.34\cdot10^{-5}$

mesh #	$x_{\min}$	$y_{\min}$	$\psi_{\min}$	$x_{\max}$	$y_{\max}$	$\psi_{\max}$
1	0.500	0.809	$-6.74\cdot10^{-2}$	0.000	0.750	$8.67\cdot10^{-19}$
2	0.598	0.731	$-9.65\cdot10^{-2}$	0.908	$9.16\cdot10^{-2}$	$7.49\cdot10^{-5}$
3	0.611	0.759	-0.102	0.960	$9\cdot10^{-2}$	$3.08\cdot10^{-5}$
4	0.614	0.731	-0.103	0.941	$5.9\cdot10^{-2}$	$1.59\cdot10^{-5}$
5	0.614	0.741	-0.103	0.941	$5.82\cdot10^{-2}$	$1.35\cdot10^{-5}$
6	0.616	0.737	-0.104	0.944	$6.48\cdot10^{-2}$	$1.29\cdot10^{-5}$

Table 12 Stream function table : Triangular meshes, $\nu = 1/100$ (top: (c1), bottom: (c2))

mesh #	$x_{\min}$	$y_{\min}$	$\psi_{\min}$	$x_{\max}$	$y_{\max}$	$\psi_{\max}$
1	0.530	0.755	$-5.39\cdot10^{-2}$	1.000	1.000	$1.73\cdot10^{-18}$
2	0.639	0.747	$-7.38\cdot10^{-2}$	1.000	1.000	$2.17\cdot10^{-18}$
3	0.626	0.748	$-8.88\cdot10^{-2}$	0.933	$5.46\cdot10^{-2}$	$6.03\cdot10^{-5}$
4	0.623	0.745	$-9.87\cdot10^{-2}$	0.930	$6.14\cdot10^{-2}$	$2.93\cdot10^{-5}$
5	0.609	0.736	-0.102	0.936	$6.15\cdot10^{-2}$	$1.73\cdot10^{-5}$

mesh #	$x_{\min}$	$y_{\min}$	$\psi_{\min}$	$x_{\max}$	$y_{\max}$	$\psi_{\max}$
1	0.530	0.755	$-5.27\cdot10^{-2}$	1.000	1.000	$1.39\cdot10^{-17}$
2	0.639	0.747	$-7.92\cdot10^{-2}$	1.000	1.000	$4.01\cdot10^{-18}$
3	0.626	0.748	$-9.25\cdot10^{-2}$	0.952	0.121	$7.24\cdot10^{-5}$
4	0.623	0.745	-0.100	0.944	$8.91\cdot10^{-2}$	$3.23\cdot10^{-5}$
5	0.609	0.736	-0.103	0.936	$6.15\cdot10^{-2}$	$1.8\cdot10^{-5}$
6	0.617	0.735	-0.103	0.946	$6.19\cdot10^{-2}$	$1.39\cdot10^{-5}$
7	0.617	0.738	-0.103	0.941	$6.25\cdot10^{-2}$	$1.3\cdot10^{-5}$

Table 13 Stream function table : Quadrangular meshes, $\nu = 1/100$ (top: (c1), bottom: (c2))

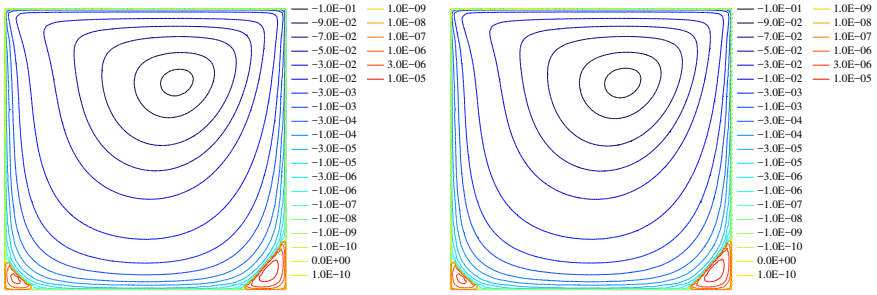

Fig. 5 Streamlines for $\nu = 1/100$ on the mesh `quad5` (left: (c1); right: (c2)).

results on the finest grids and the reference results. The good mathematical properties of this scheme can make it useful for practical applications, keeping in mind that, for simple geometries, other schemes may be more accurate and cheaper.

mesh #	$x_{\min}$	$y_{\min}$	$\psi_{\min}$	$x_{\max}$	$y_{\max}$	$\psi_{\max}$
1	0.721	0.721	$-4.21\cdot10^{-2}$	0.000	0.750	$2.17\cdot10^{-19}$
2	0.598	0.731	$-6.13\cdot10^{-2}$	0.908	$9.16\cdot10^{-2}$	$1.81\cdot10^{-4}$
3	0.594	0.675	$-8.12\cdot10^{-2}$	0.883	0.147	$6.34\cdot10^{-4}$
4	0.555	0.615	-0.105	0.884	0.136	$6.46\cdot10^{-4}$
5	0.554	0.604	-0.112	0.890	0.127	$6.4\cdot10^{-4}$

mesh #	$x_{\min}$	$y_{\min}$	$\psi_{\min}$	$x_{\max}$	$y_{\max}$	$\psi_{\max}$
1	0.501	0.499	$-3.68\cdot10^{-2}$	0.000	0.750	$1.48\cdot10^{-17}$
2	0.633	0.645	$-7.65\cdot10^{-2}$	0.908	$9.16\cdot10^{-2}$	$2.55\cdot10^{-4}$
3	0.590	0.628	$-9.99\cdot10^{-2}$	0.883	0.147	$7.72\cdot10^{-4}$
4	0.555	0.615	-0.111	0.883	0.120	$6.87\cdot10^{-4}$
5	0.554	0.604	-0.114	0.880	0.121	$6.6\cdot10^{-4}$
6	0.556	0.606	-0.114	0.884	0.121	$6.49\cdot10^{-4}$

Table 14 Stream function table : Triangular meshes, $\nu = 1/400$ (top: (c1), bottom: (c2))

mesh #	$x_{\min}$	$y_{\min}$	$\psi_{\min}$	$x_{\max}$	$y_{\max}$	$\psi_{\max}$
1	0.530	0.755	$-3\cdot10^{-2}$	1.000	1.000	$1.73\cdot10^{-18}$
2	0.639	0.747	$-4.41\cdot10^{-2}$	1.000	1.000	$1.64\cdot10^{-17}$
3	0.626	0.748	$-5.9\cdot10^{-2}$	0.952	0.121	$1.3\cdot10^{-4}$
4	0.588	0.664	$-8.03\cdot10^{-2}$	0.907	0.152	$4.42\cdot10^{-4}$
5	0.562	0.624	$-9.86\cdot10^{-2}$	0.891	0.140	$5.96\cdot10^{-4}$

mesh #	$x_{\min}$	$y_{\min}$	$\psi_{\min}$	$x_{\max}$	$y_{\max}$	$\psi_{\max}$
1	0.530	0.755	$-2.72\cdot10^{-2}$	1.000	1.000	$1.21\cdot10^{-17}$
2	0.639	0.747	$-4.68\cdot10^{-2}$	1.000	1.000	$7.91\cdot10^{-18}$
3	0.611	0.679	$-6.56\cdot10^{-2}$	0.923	0.196	$4.36\cdot10^{-4}$
4	0.565	0.623	$-8.81\cdot10^{-2}$	0.881	0.152	$7.38\cdot10^{-4}$
5	0.561	0.608	-0.104	0.875	0.126	$6.68\cdot10^{-4}$
6	0.555	0.609	-0.111	0.883	0.125	$6.5\cdot10^{-4}$
7	0.555	0.605	-0.113	0.887	0.125	$6.45\cdot10^{-4}$

Table 15 Stream function table : Quadrangular meshes, $\nu = 1/400$ (top: (c1), bottom: (c2))

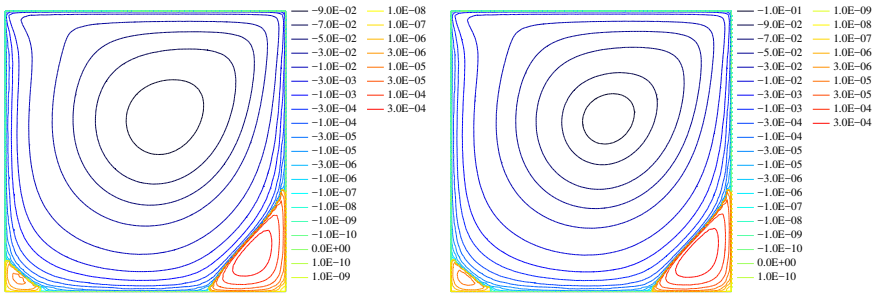

Fig. 6 Streamlines for $\nu = 1/400$ on the mesh `quad5` (left: (c1); right: (c2)).

Acknowledgements We thank the Australian Research Council's Discovery Projects funding scheme (project number DP170100605) for partially supporting this work.

References

1. Boyer, F., Omnes, P.: Benchmark for the FVCA8 Conference Finite volume methods for the Stokes and Navier–Stokes equations. In: Finite Volumes for Complex Applications VIII. Springer (2017)
2. Brezzi, F., Lipnikov, K., Simoncini, V.: A family of mimetic finite difference methods on polygonal and polyhedral meshes. Math. Models Methods Appl. Sci. **15**(10), 1533–1551 (2005)
3. Bruneau, C.H., Saad, M.: The 2d lid-driven cavity problem revisited. Computers & Fluids **35**, 326–348 (2006)
4. Chen, Z.: Equivalence between and multigrid algorithms for nonconforming and mixed methods for second-order elliptic problems. East-West J. Numer. Math. **4**(1), 1–33 (1996)
5. Droniou, J., Eymard, R.: A mixed finite volume scheme for anisotropic diffusion problems on any grid. Numer. Math. **105**(1), 35–71 (2006)
6. Droniou, J., Eymard, R.: Study of the mixed finite volume method for Stokes and Navier-Stokes equations. Numer. Methods Partial Differential Equations **25**(1), 137–171 (2009). DOI 10.1002/num.20333. URL http://dx.doi.org/10.1002/num.20333
7. Droniou, J., Eymard, R., Feron, P.: Gradient Schemes for Stokes problem. IMA J. Numer. Anal. **36**(4), 1636–1669 (2016). DOI 10.1093/imanum/drv061. URL http://dx.doi.org/10.1093/imanum/drv061
8. Droniou, J., Eymard, R., Gallouët, T., Guichard, C., Herbin, R.: The gradient discretisation method: A framework for the discretisation and numerical analysis of linear and nonlinear elliptic and parabolic problems (2016). URL https://hal.archives-ouvertes.fr/hal-01382358 (version 3)
9. Droniou, J., Eymard, R., Gallouët, T., Herbin, R.: A unified approach to mimetic finite difference, hybrid finite volume and mixed finite volume methods. Math. Models Methods Appl. Sci. **20**(2), 265–295 (2010). DOI 10.1142/S0218202510004222. URL http://dx.doi.org/10.1142/S0218202510004222
10. Droniou, J., Eymard, R., Gallouët, T., Herbin, R.: Gradient schemes: a generic framework for the discretisation of linear, nonlinear and nonlocal elliptic and parabolic equations. Math. Models Methods Appl. Sci. (M3AS) **23**(13), 2395–2432 (2013)
11. Eymard, R., Feron, P., Guichard, C.: Family of convergent numerical schemes for the incompressible Navier-Stokes equations (2016). URL https://hal.archives-ouvertes.fr/hal-01382924. Working paper or preprint
12. Eymard, R., Gallouët, T., Herbin, R.: Discretization of heterogeneous and anisotropic diffusion problems on general nonconforming meshes SUSHI: a scheme using stabilization and hybrid interfaces. IMA J. Numer. Anal. **30**(4), 1009–1043 (2010). DOI 10.1093/imanum/drn084. URL http://dx.doi.org/10.1093/imanum/drn084
13. Latché, J.C.: Personal communication (2015)
14. Liska, R., Shashkov, M., Ganza, V.: Analysis and optimization of inner products for mimetic finite difference methods on triangular grid. Math. Comput. Simu. **67**, 55–66 (2004)